

The faint outer regions of the Pegasus Dwarf Irregular galaxy: a much larger and undisturbed galaxy

Alexei Y. Kniazev,^{1,2*} Noah Brosch,³ G. Lyle Hoffman,⁴ Eva K. Grebel,⁵
Daniel B. Zucker,^{6,7,8} Simon A. Pustilnik^{9,10}

¹South African Astronomical Observatory, PO Box 9, 7935, Cape Town, South Africa

²Southern African Large Telescope Foundation, PO Box 9, 7935, Cape Town, South Africa

³The Wise Observatory and the Raymond and Beverly Sackler School of Physics and Astronomy, the Faculty of Exact Sciences, Tel Aviv University, Tel Aviv 69978, Israel

⁴Department of Physics, Lafayette College, Easton, PA 18042, USA

⁵Astronomisches Rechen-Institut, Zentrum für Astronomie der Universität Heidelberg, Mönchhofstr. 12–14, D-69120 Heidelberg, Germany

⁶Institute of Astronomy, University of Cambridge, Madingley Road, Cambridge CB3 0HA, United Kingdom

⁷Department of Physics, Macquarie University, North Ryde, NSW 2109, Australia

⁸Anglo-Australian Observatory, PO Box 296, Epping, NSW 1710, Australia

⁹Special Astrophysical Observatory, Nizhnij Arkhyz, Karachai-Circassia, 369167, Russia

¹⁰Isaac Newton Institute of Chile, SAO Branch, Nizhnij Arkhyz, Russia

Accepted 2009 August ??; Received 2009 July 31; in original form 20?? October ??

ABSTRACT

We investigate the spatial extent and structure of the Pegasus dwarf irregular galaxy using deep, wide-field, multicolour CCD photometry from the Sloan Digital Sky Survey (SDSS) and new deep HI observations. We study an area of ~ 0.6 square degrees centred on the Pegasus dwarf that was imaged by SDSS. Using effective filtering in colour-magnitude space we reduce the contamination by foreground Galactic field stars and increase significantly the contrast in the outer regions of the Pegasus dwarf.

Our extended surface photometry, reaches down to a surface brightness magnitude $\mu_r \simeq 32$ mag arcsec⁻². It reveals a stellar body with a diameter of ~ 8 kpc that follows a Sérsic surface brightness distribution law, which is composed of a significantly older stellar population than that observed in the ~ 2 kpc main body. The galaxy is at least five times more extended than listed in NED. The faint extensions of the galaxy are not equally distributed around its circumference; the north-west end is more jagged than the south-east end. We also identified a number of stellar concentrations, possibly stellar associations, arranged in a ring around the main luminous body.

New HI observations were collected at the Arecibo Observatory as part of the ALFALFA survey. They reveal an HI distribution somewhat elongated in RA and about 0.3° wide, with the region of highest column density coincident with the luminous galaxy. The HI rotation curve shows a solid-body rotation behaviour, with opposite ends differing by 15 km s⁻¹. There is a stream to lower velocities about 5 arcmin from the centre of the galaxy.

We were able to measure *ugriz* colours in a number of apertures using the SDSS data and compared these with predictions of evolutionary synthesis models. The results indicate that the outermost regions of PegDIG are 5–10 Gyr old, while the inner kpc contains stars ~ 1 Gyr old and younger. The colours correspond to K-stars; earlier subclasses are located in the innermost parts of the galaxy. PegDIG appears to be a relatively low-mass object, with a total dynamical mass of $3 \times 10^8 M_\odot$ of which only 30% in stars and 2% is in neutral gas.

The extended stellar distribution, the appearance of faint light extensions, and the lack of low column density HI tails rule out a possible tidal origin or a ram pressure stripping scenario. We propose that PegDIG is a fairly recent acquisition by the Local Group, since it does not appear to be disturbed by interactions with other galaxies.

Key words: galaxies: dwarf – galaxies: individual (Pegasus) – galaxies: structure – Local Group

1 INTRODUCTION

The Local Group (LG), our immediate neighbourhood, is the group of galaxies in which our Milky Way galaxy formed and is evolving. The Milky Way and M31 are the two dominant spiral galaxies in the Local Group, and each is surrounded by an entourage of lower-mass companions. This kind of a binary structure is found in nearby galaxy groups as well (e.g., Karachentsev et al. 2002a,b, 2003). Apart from the late-type spiral M33, the more than fifty galaxies forming the LG are either dwarf elliptical (dE), dwarf spheroidal (dSph) or dwarf irregular (dIrr) galaxies. Grebel (2001) characterised galaxies as dwarf galaxies if their total B-band or V-band magnitude is fainter than -18 mag. While the primary distinguishing feature between dIrrs and dSphs is whether they have or do not have H I, there are other distinguishing features. dIrr galaxies typically have central surface brightnesses of $\mu_{V,0} \leq 23$ mag arcsec $^{-2}$ and total H I masses $M_{HI} \leq 10^9 M_{\odot}$. As their name suggests, their optical appearance is irregular, which tends to be caused by scattered H II regions for the more massive dIrrs. They are mainly found at larger distances from massive galaxies. dEs are spherical or elliptical in appearance, typically with $M_V \geq -17$ mag, and have $\mu_{V,0} \leq 21$ mag arcsec $^{-2}$ and $M_{HI} \leq 10^8 M_{\odot}$. Along with the dSphs, they are usually found in the vicinity of massive galaxies. dSphs tend to have $M_V \geq -14$ mag, $\mu_{V,0} \geq 22$ mag arcsec $^{-2}$, and $M_{HI} \leq 10^5 M_{\odot}$. See Grebel (2001) for further details.

Dwarf galaxies are, in principle, simpler systems than large galaxies. However, those objects studied in detail showed that even dwarf systems are complex in terms of their extended star formation histories and chemical evolution (e.g., Grebel 1997; Mateo 1998). Moreover, in the LG there is evidence for past interactions among some of its galaxies, including the accretion of dwarf galaxies by the two large spirals (e.g., Ibata et al. 1994, 2001; Yanny et al. 2003; Zucker et al. 2004; Belokurov et al. 2007a; Bell et al. 2008).

The LG member galaxies reside currently in a volume with a radius of $\sim 1 - 1.2$ Mpc and their integrated mass is estimated to be between $(1.3 \pm 0.3) \times 10^{12}$ to $(2.3 \pm 0.6) \times 10^{12} M_{\odot}$ (Courteau & van den Bergh 1999; Karachentsev et al. 2002c). The LG is the best-studied galaxy group thus far and includes the faintest dwarf galaxies ever detected (e.g., Zucker et al. 2006; Belokurov et al. 2006, 2007b). The dwarf, low-luminosity bodies in the LG all contain old populations (Grebel & Gallagher 2004) and may represent relics from the re-ionisation epoch (Gnedin & Kravtsov 2006). Finally, there are persistent claims that dwarf galaxies are dark-matter (DM) dominated. Studying their properties in the LG, the place where the most detailed work can be done, is a step toward understanding the nature of DM (e.g., Gilmore et al. 2007).

It is important to determine how large a galaxy is in any observational band. The apparent size alters the baryonic mass estimate and shows how extended the stellar component is in comparison to the gas. This has also implications on the possible evolution of the object, because the larger a galaxy's cross-section, the higher are its chances of having interacted with other galaxies since its formation. The shape of the outer regions of a galaxy is a particularly sensitive indicator of past interactions; these tend to strip away

stars and ISM creating tidal tails and spreading debris in the vicinity of a galaxy. However, it is very difficult to determine the morphology of the outer extremely faint surface brightness regions for galaxies in the LG. Their closeness implies a large angular extent. If the coverage of faint surface brightness levels over large areas is required, the necessary observing time for direct, wide-field imaging becomes prohibitive. In addition, it is important to note that distorted galaxy shapes at low light levels can be an artefact of Poisson scatter (Martin, de Jong, & Rix 2008).

The availability of imaging data from the Sloan Digital Sky Survey (SDSS, York et al. 2000; Stoughton et al. 2002) offers a new and different way to approach this task. This data set is very uniform, covers a large fraction of the sky in five spectral bands, reaches objects as faint as 24 mag, and is publicly available. The SDSS imaging data have already used to explore the structural parameters of other LG objects (e.g., Draco: Odenkirchen et al. (2001b), And IX: Zucker et al. (2004); And X: Zucker et al. (2007); Ursa Major: Willman et al. (2005); Leo II: Coleman et al. (2007), and many others).

In this paper we present a new interpretation of observational material of the Pegasus dwarf irregular galaxy (DDO 216=UGC 12613, hereafter referred to as PegDIG) based on very deep and wide-field surface photometry using imaging data from the SDSS. PegDIG is one of the fainter LG members and contains very few stars younger than 100 Myr (see also Gallagher et al. 1998). This object is not to be confused with the dwarf spheroidal galaxy Pegasus II = Peg dSph = Andromeda VI (Karachentsev & Karachentseva 1999; Grebel & Guhathakurta 1999; Armandroff et al. 1999).

We trace PegDIG across its entire angular extent in the optical to the lowest accessible surface brightness levels using SDSS data, since all previous studies concentrated either on stars near the centre of the galaxy (e.g., Gallagher et al. 1998) or presented surface brightness profiles covering only small fields (e.g., van Zee 2000). We combine these data with new H I maps derived from Arecibo Observatory¹ data collected for the ALFALFA survey (e.g., Haynes et al. 2008).

2 THE PEGASUS DWARF IRREGULAR GALAXY

As discussed by Gallagher et al. (1998), PegDIG exhibits many of the properties typical of dIrr galaxies such as H I, young stars, and H II regions, and an irregular appearance due to recent star formation. On the other hand, it is at the faint end of the luminosity range of dIrrs, its outer isophotes are fairly smooth, its gas content is comparatively low, and its recent star formation activity is low as well, prompting Gallagher et al. (1998) to suggest that it may be a dIrr/dSph transition-type galaxy.

¹ The Arecibo Observatory is part of the National Astronomy and Ionosphere Center, which is operated by Cornell University under a cooperative agreement with the National Science Foundation.

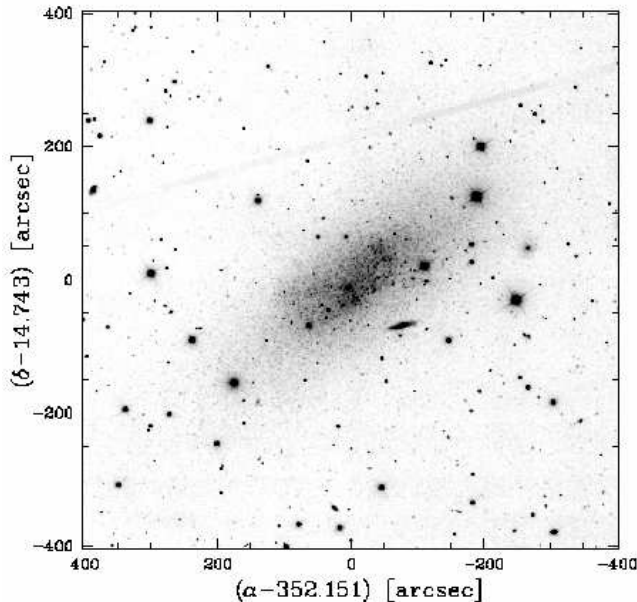


Figure 1. The central part ($\sim 13.5 \times 13.5$ arcmin) of combined g , r , and i image of Pegasus dwarf galaxy derived from a weighted combination of individual single-colour images from the SDSS. North is up and East is to the left. The oblique faint line is a satellite track that was registered on the SDSS r image. At the adopted distance of 1.0 Mpc, $1'' = 4.85$ pc.

2.1 Optical data, morphology, star formation and distance estimates

The basic parameters of PegDIG, compiled from the literature, are listed in Table 1. There has been significant disagreement among the various distance estimators presented in the past, ranging from 1.75 Mpc derived from Cepheids to 760 kpc derived from the tip of the red giant branch (TRGB) in colour-magnitude diagrams. de Vaucouleurs (1975) quoted a distance of only 170 kpc to PegDIG, considering the galaxy one of our closest neighbours. The three most recent determinations all use ground-based photometric data and employ the TRGB (McConnachie et al. 2005; Tikhonov 2006a) or Cepheids (Meschin et al. 2009) as distance indicators. These studies converge to a value of about 1 Mpc, slightly larger than the distance of 760 ± 100 kpc derived by Gallagher et al. (1998) using data from the Hubble Space Telescope. These distances render PegDIG a peripheral, potential member of the M31 subgroup within the LG. We adopt here a nominal distance to PegDIG of 1 Mpc.

Gallagher et al. (1998) studied the central region of PegDIG using imaging in the B, V and I bands with the Wide Field and Planetary Camera (WFPC2) aboard the Hubble Space Telescope (HST). Their field encompasses regions of recent SF in PegDIG. These authors obtained the deepest photometry of PegDIG so far, reaching objects down to $V \simeq 25$. They identified a main sequence as well as blue loop stars younger than 0.5 Gyr. These young populations are clustered in two central clumps. Moreover, there are older, more widely distributed stars. Gallagher et al. (1998) and Dohm-Palmer et al. (1998) concluded that the model best fitting their measurements has a relatively constant SF

rate over several Gyrs, with a period of enhanced SF about 2 Gyrs ago. The colours of the main-sequence stars measured by Gallagher et al. (1998) indicate a relatively high extinction of $A_V \simeq 0.47$ or $E(B - V) = 0.15$, and the stellar models could match the observations only for a distance to PegDIG of 760 kpc. Gallagher et al. (1998) combined various measurements including the H I column density and IRAS dust maps in order to constrain the reddening and pointed out that these estimators do not yield consistent results. The adopted extinction is one of the main reasons for their shorter distance.

Krienke & Hodge (2001) used the colours and redshifts of background galaxies visible in the HST/WFPC2 data of Gallagher et al. (1998) to estimate the internal reddening in the central region of PegDIG. After correcting for the Galactic foreground reddening using the values of Schlegel et al. (1998), they found that PegDIG itself contributes very little to the reddening and seems to have hardly any interstellar dust. Krienke & Hodge (2001) derived an internal reddening of $E(B - V) \leq 0.03$ for PegDIG, consistent with Gallagher et al. (1998). The total reddening of Krienke & Hodge (2001) is lower than that of Gallagher et al. (1998) by ≥ 0.05 in $E(B - V)$.

Young et al. (2003) estimated a current star formation rate of $3 \times 10^{-5} M_{\odot} \text{ yr}^{-1}$ from the H α flux, based on the broadband and H α imaging in van Zee (2000). Hunter & Elmegreen (2004) listed PegDIG as having the lowest star formation rate among the 94 irregular galaxies of their sample ($4.4 \times 10^{-5} M_{\odot} \text{ yr}^{-1}$) and the lowest star formation rate per surface area ($8.3 \times 10^{-4} M_{\odot} \text{ yr}^{-1} \text{ kpc}^{-2}$).

NED lists a major axis of 5 arcmin (~ 1.5 kpc at 1 Mpc) and a minor axis of 2.7 arcmin for PegDIG. Tikhonov (2006a) found a 5 kpc thick disk (diameter ~ 16 arcmin at 1 Mpc) by tracing the red giant stars on images obtained with the 6-m BTA telescope and with HST. He wrote that the low-luminosity blue stars in PegDIG are scattered throughout the $5' \times 3'$ body of the galaxy. The HST image allowed the decomposition of the blue star distribution perpendicular to the disk; these stars “virtually disappear at 200 pc” while the thick disk can be traced vertically to ~ 1 kpc.

Recently, McConnachie et al. (2007) compared the stellar structure of PegDIG derived from Johnson V and Gunn i images from the INT Wide Field Camera with the H I maps produced by Young et al. (2003). They concluded that the H I distribution is different from that of the “regular, elliptical” stellar distribution, and interpreted that as strong evidence for ram-pressure stripping of the PegDIG by an intergalactic medium associated with the Local Group.

2.2 The interstellar matter: HI distribution, mass, and dynamics

Fisher & Tully (1975) were the first to detect H I emission from PegDIG and, based on its low radial velocity, suggested it is a Local Group member. The 21-cm line emission they measured had a width of $43 \pm 7 \text{ km sec}^{-1}$. The neutral hydrogen in PegDIG was mapped by Lo, Sargent, & Young (1993) with the VLA, and by Hoffman et al. (1996) with the Arecibo radio telescope. Lo et al. (1993) showed that the H I is concentrated in the main optical body and that it shows some clumps. Hoffman et al. (1996) found that the H I distribution was asymmetric, with the H I peak offset

Table 1. Basic Parameters of the Pegasus Dwarf Irregular Galaxy

Parameter (1)	Value (2)	Reference (3)	
α (J2000.0)	$23^h 28^m 36.25^s$		
δ (J2000.0)	$+14^\circ 44' 34.5''$		
B_T (mag)	12.50 ± 0.15	van Zee (2000)	
$(B - V)$ (mag)	0.64 ± 0.04	van Zee (2000)	
$(U - B)$ (mag)	0.00 ± 0.09	van Zee (2000)	
α_B (arcsec)	104.4	van Zee (2000)	
Distance estimates			
Method (1)	Distance Modulus (2)	kpc (3)	Reference (4)
PN		200–1600	Jacoby & Lesser (1981)
TRGB	≈ 26	1700	Hoessel & Mould (1982)
TRGB	≈ 25.5	700–1200	Christian & Tully (1983)
Cepheids	26.1 ± 0.3	1700	Hoessel et al. (1990)
TRGB	24.9 ± 0.1	950 ± 50	Aparicio (1994)
TRGB	25.13 ± 0.11	1060 ± 50	Lee (1995)
TRGB, RC	24.40	760 ± 100	Gallagher et al. (1998)
TRGB	24.80 ± 0.07	919 ± 30	McConnachie et al. (2005)
TRGB	25.04	1020 ± 20	Tikhonov (2006a)
Cepheids		1070 ± 50	Meschin et al. (2009)

Note: The abbreviations used here are as follows: α_B is the exponential scale length of the disk fitted by van Zee (2000) to the B surface brightness profile; PN refers to a distance estimate using planetary nebulae; TRGB is a distance using the tip of the red giant branch in the colour-magnitude diagram; RC is the same, but using the “red clump”.

by $\sim 1'$ from the centre of the outer iso-intensity contour. The rotation curve derived from the Arecibo observations becomes flat at about ~ 4.5 arcmin SE of the kinematic centre, which is itself offset by ~ 2.6 arcmin from the optical centre. On the NW side the rotation curve falls off after peaking at ~ 2 arcmin from the kinematic centre. Note that Young et al. (2003) mention that the low velocity of PegDIG very close to zero – causes significant confusion with Galactic H I, thus the interpretation of single-dish wide-beam H I measurements of this galaxy may be problematic.

Karachentsev, Karachentseva, & Huchtmeier (2001) observed PegDIG with the Effelsberg radio telescope as part of a program to map the local galaxy population. They give only an upper limit of 11 mJy from the H I line flux, which they attribute to a low H I content and not to confusion from local H I. Note that the 21-cm half-power beam at Effelsberg is 9.3 arcmin.

van Zee (2000) reported results of a study of isolated dwarf galaxies, where “isolated” implies a distance of 100–200 kpc from the nearest neighbour, using UBV and $H\alpha$ imaging, combined with VLA H I mapping. PegDIG was included in her sample and yielded an integrated flux of 29.90 Jy km s $^{-1}$ and an H I line width of 40 km s $^{-1}$ for a recession velocity of -183 km s $^{-1}$, based on the VLA observations reported in Young et al. (2003). van Zee’s (2000) photometry showed that PegDIG has the reddest colours of all galaxies in her sample. Evolutionary synthesis models indicate that the stellar population could be the result of a single major star formation (SF) burst a few Gyr ago that ran out of material for further SF.

Further H I mapping of PegDIG was done at Westerbork by Stil & Israel (2002), as part of a project to study the hydrogen in a sample of dwarf galaxies. PegDIG was

considered by these authors as one of their most isolated objects. Stil & Israel (2002) found a 9.0 mJy upper limit to the 1.4 GHz continuum flux from the galaxy in the 1.35 MHz band, and a 21-cm line flux integral of 16.3 ± 0.5 Jy km s $^{-1}$, implying a total H I content of $4 \times 10^6 M_\odot$ at the assumed 1 Mpc distance. The map they presented in their Fig. 4 shows the H I concentrated at $\alpha(2000) = 23^h 26^m 04^s$ and $\delta(2000) = +14^\circ 27' 40''$, although the $13''$ synthesised beam was rather elongated in the north-south direction because of the declination of the object. The line profile shown in their Fig. 2 is single-peaked and very narrow, with a FWHM of less than 20 km s $^{-1}$ and a weak ~ 80 km s $^{-1}$ tail to higher recession velocities (the systemic H I velocity of the galaxy being -189 km s $^{-1}$).

The most recent published H I map of PegDIG was by Young et al. (2003) using the VLA and combining observations performed in the C and D configurations. Their integrated 21-cm profile has a 50% full width of 24.6 km s $^{-1}$ and a flux integral of 29.9 Jy km s $^{-1}$. Young et al. (2003) display in their Fig. 5 a contour map of PegDIG with the lowest column density level at 10^{19} atoms cm $^{-2}$ and a ~ 10 arcmin extent that shows the gas arranged in three main clumps. In addition, a region 1.5 arcmin northwest of the centre shows a double H I profile; this is interpreted as an expanding bubble with a radius of one arcmin (≈ 200 pc at the 760 kpc assumed distance).

Jackson et al. (2006) presented spatially-resolved maps of PegDIG at 4.5 and 8 μ m obtained with the Spitzer IRAC camera. These maps show only low surface brightness emission from the galaxy, indicating low amounts of hot dust grains and PAHs in the ISM. This, Jackson et al. (2006) propose, is the result of the destruction of grains by super-

Table 2. Photometric parameters for the unresolved part of PegDIG in the SDSS

Filter	Circular Apertures				2D GALFIT		
	b/a	μ_0 [mag/sq.arcsec]	α [arcsec]	n	b/a	r_e [arcsec]	n
(1)	(2)	(3)	(4)	(5)	(6)	(7)	(8)
<i>u</i>	0.40	24.24±0.10	89±9	1.05±0.05	0.40±0.01	172: (98:)	0.96±0.04
<i>g</i>	0.40	23.10±0.05	98±5	1.03±0.02	0.40±0.01	172±1 (108)	1.04±0.02
<i>r</i>	0.40	22.73±0.04	114±5	1.10±0.02	0.41±0.01	172±1 (126)	1.18±0.02
<i>i</i>	0.40	22.46±0.05	118±5	1.11±0.03	0.39±0.01	177±1 (139)	1.25±0.02
<i>z</i>	0.40	22.40±0.07	127±7	1.33±0.06	0.40±0.01	164±2 (125)	1.22±0.02

Table 3. Total magnitudes of the Pegasus dwarf irregular galaxy

Filter	Circular Apertures		2D GALFIT	A_λ
	Apparent [mag]	Total [mag]	Total [mag]	[mag]
(1)	(2)	(3)	(4)	(5)
<i>u</i>	13.64±0.03	13.60±0.46	13.20±0.03	0.34
<i>g</i>	12.26±0.02	12.23±0.20	12.01±0.02	0.25
<i>r</i>	11.67±0.02	11.63±0.17	11.48±0.02	0.18
<i>i</i>	11.35±0.02	11.32±0.21	11.16±0.02	0.14
<i>z</i>	11.37±0.03	11.32±0.29	11.08±0.03	0.10
<i>(u - g)</i>		1.37±0.50	1.19±0.04	
<i>(g - r)</i>		0.60±0.26	0.53±0.03	
<i>(r - i)</i>		0.31±0.27	0.32±0.03	
<i>(i - z)</i>		0.00±0.36	0.08±0.04	
<i>U</i>		12.88	12.49±0.05	0.36
<i>B</i>		12.68	12.43±0.03	0.28
<i>V</i>		11.87	11.69±0.03	0.22
<i>R_c</i>		11.41	11.27±0.04	0.18
<i>I_c</i>		10.89	10.74±0.05	0.13

nova shocks and the inability of the ISM to regrow them in a regime of low or zero star formation rates.

3 THE SDSS DATA FOR THE PEGASUS DWARF IRREGULAR GALAXY

An image of PegDIG was created by extracting the relevant area from the SDSS data release DR5 (Adelman-McCarthy et al. 2007) imaging data set. Owing to the distance of PegDIG, the high stellar densities in its central regions, and an average seeing of $\sim 1.5''$ in the SDSS imaging data, individual stars can no longer be resolved as point sources in this area. We performed surface photometry separately for the inner galaxy parts, and for the outer parts, where stars still can be resolved. The two independently-derived surface photometry results were subsequently combined into a single, global surface photometry profile using areas of overlap. The results for the outer part were matched to those for the inner part, yielding a single surface brightness profile (SBP) per band for the entire galaxy.

3.1 Integrated photometry and Surface Brightness Profiles

PegDIG itself was not identified as a separate entity by the standard SDSS pipeline (see, for example, the SDSS DR6 database). The integrated photometry, the creation of SBPs, and their analysis were done in the manner described in detail by Kniazev et al. (2004). First, *g*, *r* and *i* images for a wide region around the galaxy were extracted from the SDSS database. These were combined with weights to form an image of the object that is deeper than any of the single SDSS bands could offer and that has essentially the same stellar point spread function ($\text{FWHM} \simeq 1''$) as the pipeline-reduced SDSS data. The central part of the combined *gri* image is shown in Figure 1. The galaxy location was defined above the 3σ noise level on the smoothed combined image, and all background sources were subtracted using SDSS database coordinates and using additional masking. The background was subtracted and SBPs for all *ugriz* filters were created in circular apertures with a uniform isophote step size of $2''$. The calculated profiles were fitted on a logarithmic scale, following Sérsic (1968):

$$\mu(r) = \mu_0 + 1.086 \cdot (r/\alpha)^n, \quad (1)$$

where R is the distance along the axis and n is an additional parameter.

To check the stability of our results we performed additional two-dimensional modelling with the GALFIT program (Peng et al. 2002) using a one-component Sérsic function for all *ugriz* filters. To exclude all foreground stars from the fitting procedure we used the same mask image that was calculated on the previous step, where the method of circular apertures was used.

The results for both methods are summarised in Tables 2 and 3. Table 2 presents all the model parameters for both methods, except for the total magnitudes. In case of circular apertures, the b/a axis ratio was calculated only once when building the mask for the galaxy location and was kept constant for the different filters. When GALFIT was used, the b/a axis ratio was allowed to vary as one of the parameters of the fitted model. GALFIT uses the following form for the Sérsic function:

$$\mu(r) = \mu_e + \left\{ -b_n \left[\left(\frac{r}{r_e} \right)^n - 1 \right] \right\} \quad (2)$$

where μ_e is the effective surface brightness and r_e is the effective (half-light) radius. Generally $\alpha = r_e/b_n$, but b_n is different for each n and can be only found numerically. A good

approximation that can be used is $b_n \sim 2/n - 0.324$, but this is valid only for $0.07 \leq n \leq 1$ (Trujillo, Graham, & Caon 2001) and is not correct here, since $n > 1$. For this reason, our recalculations from r_e to α are presented in brackets in column 7 (r_e) of Table 2. The GALFIT solution for the u filter was unstable and for this reason we fixed r_e to the same value it was for g . This parameter is marked with a colon.

Table 3 presents the total magnitudes. In column 2, the apparent magnitudes derived by integrating the luminosity within a circular aperture out to the limiting isophotal level of the SDSS data are listed. The total magnitudes presented in Table 3 were calculated extrapolating out to $r = \infty$ using equation (9) from Kniazev et al. (2004) and the parameters of the Sérsic function listed in Table 2. The rather large errors of these magnitudes result from the big errors of the input parameters in Table 2. The total magnitudes from GALFIT are also a result of flux integration out to $r = \infty$. In the case of GALFIT, the total magnitude is a free parameter of the fit. We also presented $UBVR_cI_c$ magnitudes that were recalculated from the $ugriz$ magnitudes using of equations from Jordi, Grebel, & Ammon (2006). The magnitudes in Table 3 are not corrected for foreground Milky Way extinction, but extinction corrections calculated using the Schlegel et al. (1998) prescription are shown in column 5 of this table.

The photometric parameters calculated with either of the methods are very similar, but the total magnitudes resulting from GALFIT are systematically larger. Comparing with the integrated photometry of van Zee (2000) we note that our 2D GALFIT values for B_T , $(B - V)$ and $(U - B)$ are very similar to those of van Zee.

3.2 The Resolved Outer Part

3.2.1 Photometric selection of PegDIG stars

Tracing out PegDIG to much fainter surface brightness levels than allowed by the direct surface photometry described in the previous section is based on selecting stellar objects that probably belong to the galaxy and on rejecting those that likely belong to the foreground. This method of empirical photometric filtering was first described and used by Grillmair et al. (1995). It was first implemented for SDSS data by Odenkirchen et al. (2001a) for the globular cluster Pal 5 and was used by Odenkirchen et al. (2001b) to study the Draco dwarf spheroidal galaxy. Variants of this photometric filtering of resolved stellar point sources in the SDSS were also developed and used by Rockosi et al. (2002), Smolčić et al. (2007), and Coleman et al. (2007).

First, we selected all point sources imaged by the survey in a ~ 0.6 square degree region centred on the Pegasus dwarf galaxy. Approximately 8000 point sources in this area were classified by the standard SDSS pipeline as stars. Since the SDSS detects only the most luminous stars in PegDIG, the number of identifiable stars belonging to the galaxy is quite limited. For this reason we did not use any additional selection criteria, but rejected only the sources for which the photometric error in any of the three most sensitive passbands (gri) was larger than 0.4 mag. The spatial distribution of all the selected sources has a mean stellar density of ~ 2.85 stars

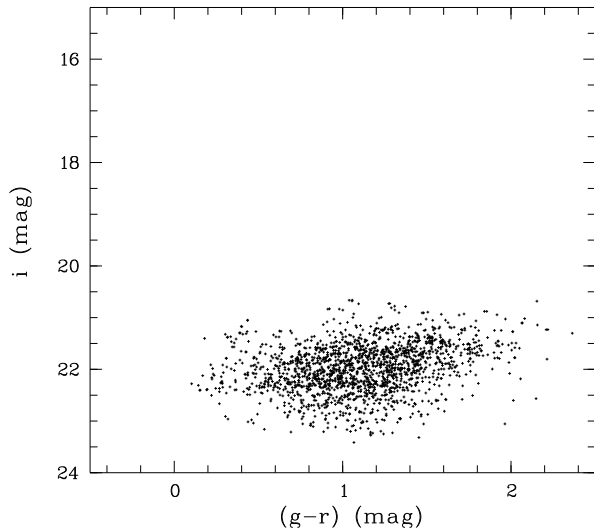


Figure 2. i versus $(g - r)$ colour-magnitude diagram for stars selected in an elliptical annulus with a semi-major axis of 0.05–0.15 deg, ellipticity 0.6 and PA= -55° , centred on $(\alpha, \delta)=(352.15^\circ, +14.743^\circ)$.

arcmin^{-2} for the foreground stars (all areas, excluding the central part of the field where PegDIG is obviously located).

The crucial point in constructing a high-contrast map for the outer part of the Pegasus system is to achieve an efficient discrimination between the tracers of this system and the foreground field stars. Following Odenkirchen et al. (2001b), we created a training set by selecting ~ 1500 stars from the central part of the PegDIG (defined as an ellipse with a semi-major axis of $0^\circ.15$, ellipticity 0.6 and PA= -55° , centred on $(\alpha, \delta)=(352.15^\circ, +14.743^\circ)$).

In Fig. 2 we show a colour-magnitude diagram of the point sources that are candidate members of PegDIG as mentioned above. The diagram shows a fairly amorphous, extended plume of faint sources that resemble the distribution of stars in other distant dIrr galaxies from early CCD observations (e.g. Tosi et al. 1991; Greggio et al. 1993). The SDSS data share several characteristics with these early, ground-based CCD data: For a galaxy at the distance of PegDIG, they are close to the detection limit and they are strongly confusion and crowding limited. The extended plume of stars in the SDSS stellar point source catalog is composed of young main-sequence stars, blue loop stars, red supergiants, luminous asymptotic giant branch stars, and stars at the tip of the red giant branch. In other words, we are sampling the most luminous stars in PegDIG, which represent a range of different stellar populations and ages covering many billions of years. While these shallow data are not suited nor intended for detailed studies of the star formation history of PegDIG, they are very valuable for studies of its structure. The fact that stars on the upper red giant branch are included is particularly important, since this will be helpful when trying to trace the faint outer limits of PegDIG, which are typically dominated by old(er) populations.

Following the procedure, described by Odenkirchen et al. (2001a,b), we calculated new colour indices c_1 and c_2 :

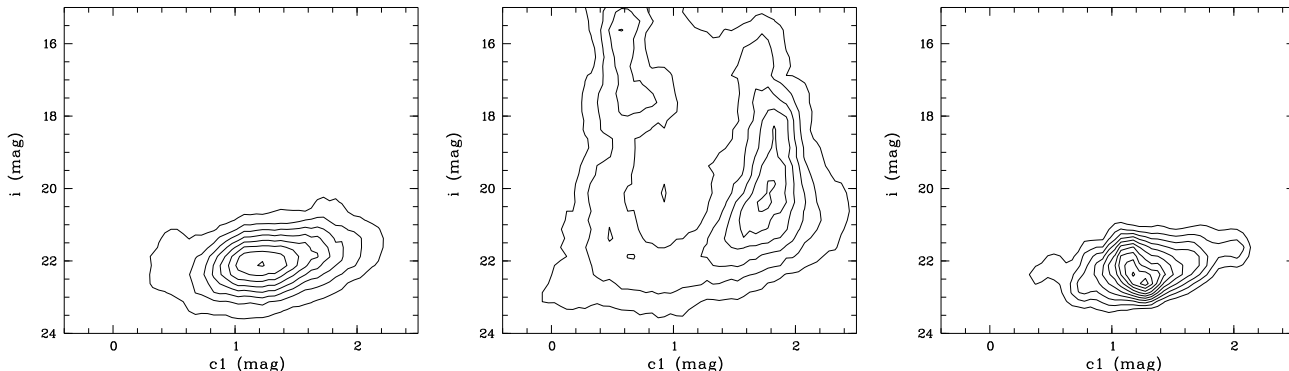


Figure 3. Separation of foreground Milky Way stars from the stars in PegDIG. *Left:* Density distribution f_P of Pegasus stars in the (c_1, i) colour-magnitude plane that is shown as contour plot. Stars were taken from an elliptical annulus as described for Fig. 2. *Middle:* Density distribution f_F of field stars in the (c_1, i) colour-magnitude plane. Stars were calculated outside of an ellipse with similar parameters and with a semi-major axis of 0.25 deg. *Right:* Lines of constant number ratio (the population contrast) $s = f_P/f_F$.

$$\begin{aligned} c_1 &= 0.921 \cdot (g - r) + 0.389 \cdot (r - i) \\ c_2 &= -0.389 \cdot (g - r) + 0.921 \cdot (r - i) \end{aligned} \quad (3)$$

The relations in the equations 3 are very close to those derived by Odenkirchen et al. (2001b) for the Draco dSph and similar to those derived by Odenkirchen et al. (2001a) for Palomar 5.

After constructing the colour index c_1 , which is a linear combination of the $(g - r)$ and $(r - i)$ colours, the next step was to design an empirical filter mask in the (c_1, i) colour-magnitude (CM) plane that will allow the optimal separation of the colour-magnitude distribution of sources belonging to the PegDIG population from that of the foreground field stars. The basic assumption is that the stars in PegDIG are of specific types, based on their colours and apparent magnitudes, and will occupy a specific locus in the CM diagram. This is shown in Figure 3. The region with maximal s values in the right panel of Figure 3 delineates the locus in the CM plane with the highest fraction of PegDIG stars relative to field stars. This last figure indicates that the stars selected from the SDSS data set as probable PegDIG members are mostly between $21 \leq i \leq 23.5$ mag.

The next step was to identify a level s_{opt} that yields the highest contrast for the selected area of PegDIG compared to the field stars. This implies that a filter mask for the selection of Pegasus stars should include as many points as possible with $s \geq s_{opt}$, where s_{opt} is a threshold value. To find the optimal number density threshold s_{opt} we computed the signal-to-noise ratio (SNR) for a range of s values, using the following equation from Grillmair et al. (1995) and from Odenkirchen et al. (2001a,b):

$$\text{SNR}(s) = \frac{N_P(s) - wN_F(s)}{\sqrt{N_P(s) + w^2N_F(s)}}, \quad (4)$$

Here $N_P(s)$ is the total number of stars in the sample defined by s and for the region of PegDIG, and $N_F(s)$ is the number of stars in the same sample, but for the region where the foreground population is probed. The w parameter scales areas of these two regions. Since we are interested in the outer part of PegDIG, the SNR was optimised first for the elliptical annulus with a semi-major axis between 0.12 and 0.20 deg from the centre of Pegasus. After that, other areas

and different foreground regions were tested; we found that s_{opt} was practically identical in all those tests.

The final selection filter constructed here removed $\sim 76\%$ of the contaminating field stars and reduced the mean density of the contaminating foreground stars from 2.85 stars arcmin^{-2} to 0.69 ± 1.67 stars arcmin^{-2} . The spatial distribution of stars identified as foreground sources is shown in the top panel of Figure 4. It is clear that these stars are randomly distributed and do not show any strong concentration toward the bright core of PegDIG; a concentration could be expected if the filtering operation had been inefficient. The spatial distribution of stars with characteristics matching our final selection filter is shown in the bottom panel of Figure 4. A visual comparison of the top and bottom panels of this figure shows that the objects selected by the filter as candidate PegDIG members do concentrate around the known galaxy, implying that the filtering operation indeed selected preferentially PegDIG stars very distant from the unresolved inner body.

A stellar number density map of the central part of the studied field is shown in Figure 5 as isopleths. The surface density was derived through counts on a $30''$ by $30''$ grid and subsequent weighted averaging within a radius of one grid step. The thin lines show contours at the 1σ level above the mean background density, where σ is the rms of the background stellar density fluctuations, showing the lowest level at which the PegDIG stars start to be recognisable. Since any significant detection of the PegDIG population requires a surface density of at least 2σ above the background, this level is marked by the thick contour in Figure 5. Levels of 3σ , 5σ and 10σ are plotted there with thick lines as well, to reveal the shape of the galaxy at different stellar number densities; the plot shows that the overall distribution of PegDIG stars is approximately ellipsoidal, but that the outer contours appear deformed. It is also obvious that the NW end of the galaxy seems to be much more irregular than the SE one. These deviations, at the NW end, are very strong, showing up even at the 3σ contour.

3.2.2 Structure of PegDIG

To quantify the size, shape and orientation of the Pegasus dwarf irregular galaxy we fitted a two-dimensional model

Table 4. Parameter values for the best-fit model for the surface density distribution of PegDIG

Model	α_c [2000.0]	δ_c [2000.0]	b/a	PA [degree]	α [arcsec]	n
2D Sérsic	23:28:35.52	+14:44:29.04	0.39 ± 0.01	$-55^\circ 7 \pm 0^\circ 1$	138 ± 2	1.11 ± 0.02
1D Sérsic			0.40	$-55^\circ 7$	192 ± 35	1.36 ± 0.21
Model	α_c	δ_c	b/a	PA	r_c	r_t
2D King 62	23:28:35.02	+14:44:28.30	0.38 ± 0.03	$-55^\circ 9 \pm 0^\circ 1$	39 ± 20	957 ± 50

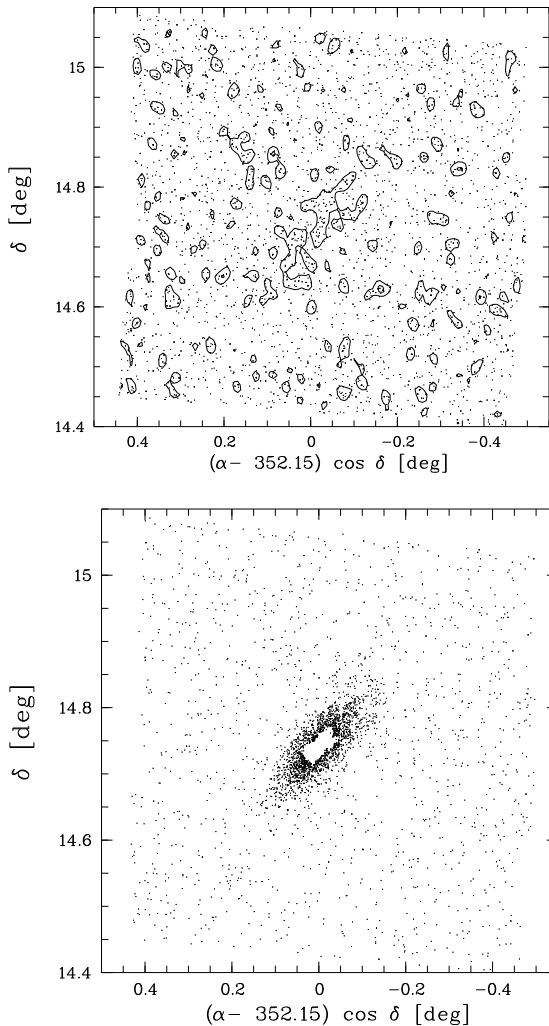


Figure 4. The spatial distribution of SDSS selected point sources in the direction of the Pegasus dwarf galaxy. *Top panel:* Stars selected by the algorithm as belonging to the Galactic foreground appear randomly distributed in this image. Contours of equal stellar surface density at a level of 1σ and 2σ are shown with thin lines (σ is the rms background variation). There are some concentrations at only a 1σ level in the center. *Bottom panel:* Final spatial distribution of ~ 3400 photometrically selected stars in the PegDIG area. The stars selected as candidate PegDIG members are concentrated around the recognised location of the galaxy.

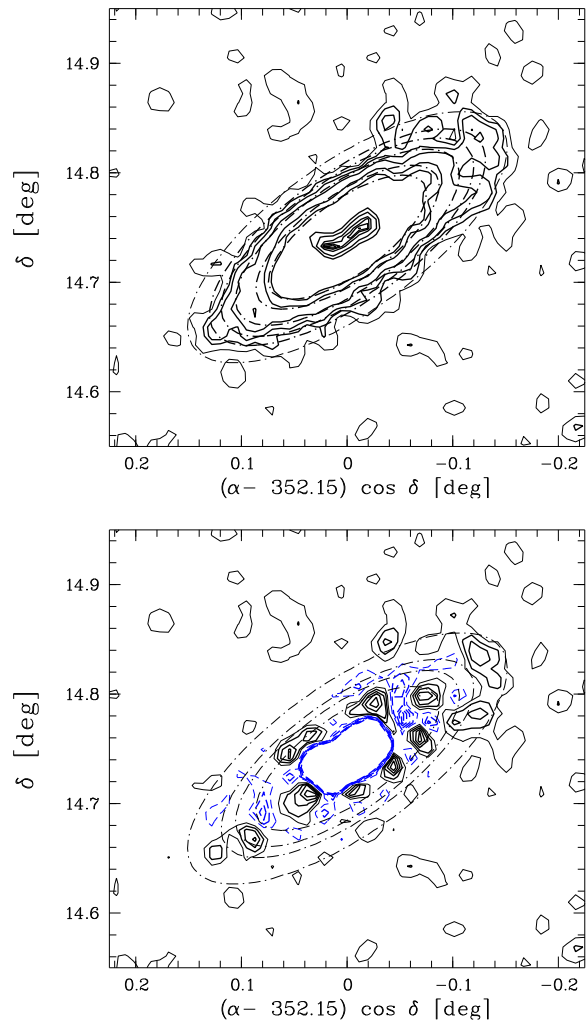


Figure 5. *Top:* Contour plots of the observed distribution of stars in PegDIG. Contours of equal stellar surface density are shown at 2σ , 3σ , 5σ and 10σ with a thinner contour at 1σ . The profiles in the centre of the galaxy show a “hole” produced by missing information in the high stellar density part of the galaxy. Dot-dashed lines show the contours of the best-fit exponential model (2D Sérsic profile) at 1σ , 3σ , 5σ and 10σ levels. Note the “dendritic” extensions of the faint contours in the north-west part of the galaxy. *Bottom:* Residuals of the fit shown in the top panel, rescaled to the level of the mean background counts. As before, the contour with thinner lines corresponds to levels of $\pm 1\sigma$. Short-dashed (blue) lines show negative levels of the residuals.

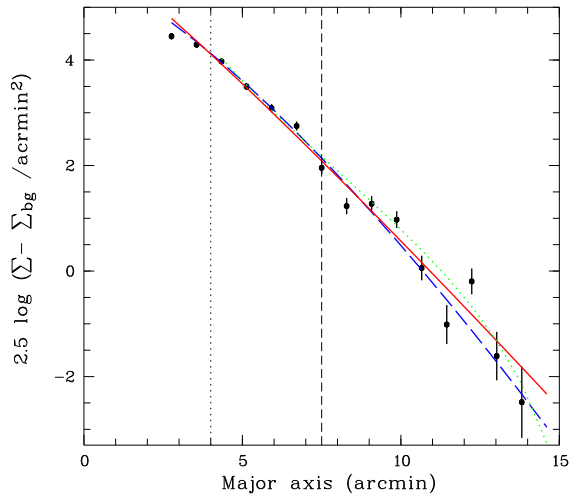


Figure 6. Radial profile of the surface density of stars in PegDIG. Data points with error bars show the profile of the observed distribution (star counts in elliptical rings around the centre of PegDIG with parameters of the best-fit model shown in Table 4, and with the mean background $0.69 \text{ stars arcmin}^{-2}$ subtracted). The red solid line shows the major axis model distribution for the GALFIT 2D Sérsic model (see Table 4 for parameters). The blue long-dashed line shows the best-fit 1D Sérsic model, where the point at $\sim 12 \text{ arcmin}$ was excluded since it represents the extensions visible in the bottom panel of Figure 5. When doing a fit with this point included, the result of the 1D fitting is very close to the result of 2D with GALFIT. The green dotted line shows the major axis model distribution for the GALFIT 2D King model (see Table 4 for parameters). Points located to the left of the vertical dotted line at $R=4 \text{ arcmin}$ were not included in the fit for either model. The vertical short-dashed line indicates a radial distance of $\sim 450 \text{ arcsec}$, where our SBP profiles in the *ugriz* filters terminate.

to the observed surface density distribution. For that, the surface density was sampled on a $30'' \times 30''$ grid of non-overlapping cells. We performed two-dimensional modelling using GALFIT with a one-component Sérsic function. The central part of the galaxy (which looks like a hole in our data) was excluded from the modelling with the special mask allowed by GALFIT. The best-fit parameters are given in Table 4 and the best fit is shown in Figures 5 and 6. The lower panel of Figure 5 shows the difference between the actual data and the fitted model.

Although the statistical significance of any single feature may not be extremely high, we note that there seems to be a ring-like distribution of peaks (clumps) around the unresolved part of the galaxy. The peaks in the ring configuration encircling the inner, unresolved part of the galaxy are highly significant, more than 5σ above the background. The three peaks revealed to the north-west of the galaxy, between the 1σ and 3σ contours of the model, are of possibly even higher significance. These peaks could not be just artefacts of Poisson noise, as suggested by Martin, de Jong, & Rix (2008) for other faint nearby galaxies, but here they are sufficiently significant, namely 3σ or higher, as shown in the lower panel of Fig. 5. Such peaks are not seen at the opposite end of the galaxy and represent deviations of the faint outskirts of the galaxy from a pure Sérsic profile, which are restricted to the NW side.

As can be seen in Figure 5, the highest density of detected stars in the area of the peaks (clumps) is about $10\text{--}20 \sigma$ of the estimated background noise scatter. With the latter value $1.67 \text{ star arcmin}^{-2}$ (see Section 3.2), the 20σ level corresponds to a star density of $33.5 \text{ star arcmin}^{-2}$ or $\sim 0.009 \text{ star arcsec}^{-2}$. In other words, the area with the highest density of detected stars in the SDSS Pegasus data corresponds to about one star in a circle with a radius of $\sim 6 \text{ arcsec}$. For an effective seeing of one arcsec and a pixel scale of 0.396 arcsec there should not be any crowding problem in the regions with this and lower stellar density, either for detection, or for object classification as a star/nebula.

To demonstrate the evidence for a much larger spatial extent of PegDIG indicated by our data, we show in Figure 6 the observed radial stellar density profiles. These were derived from star counts in elliptical annuli, with parameters of the ellipses taken from Table 4. The logarithm of the mean density above background is plotted versus the radius of each annulus. The radius refers to the distance along the fitted major axis. The central $2.7'$ region was not included in the fit and is not shown.

The best-fitting generalised Sérsic model, described by the parameters listed in Table 4, is characterised by a radial scale length of $\alpha = 138 \text{ arcsec}$ and an exponent $n = 1.11$. Comparing these numbers with those shown in Table 2 one can see that both the exponent n of the density distribution and the scale parameter α are very close to the values derived from the *gri* images. As Figure 6 shows, the model profile fits our data very well over the entire region; there is no compelling evidence for a real cutoff in the radial profile of PegDIG within the current observational limits. Using SDSS data for the unresolved part of the galaxy we can trace the galaxy only up to a $\sim 450''$ radius along the major axis. Using star counts, and improving the contrast of our density map, we can trace PegDIG up to $\sim 800''$, but a distinct edge of the galaxy still remains undetected.

The model fits provide a useful, smooth reference against which to identify peculiarities in the shape of the observed distribution of stars. Such peculiarities are the above-mentioned “ring” of stellar density peaks around the unresolved part of the galaxy, and the three peaks at the NW end of the faint galaxy extension revealed by our filtering procedure and subtraction of the fitted model. We note that there are no counterparts to these peaks in the SE part of PegDIG. These features will be discussed below.

3.2.3 Surface Brightness Profiles from Star Counts

Our filtered star count data allow us to construct surface brightness profiles (SBPs). Such SBPs can be derived using the filtered star count data, summing stellar magnitudes in elliptical annuli where the parameters of the ellipses are taken from Table 4, and normalising them to the area of the annuli.

Assuming that the PegDIG stellar populations do not vary wildly in the outer parts of the galaxy (indeed they do not, as we show below), we can conclude that one sees the same profiles regardless of the method used. In the case of the unresolved part of PegDIG these were calibrated correctly, but those constructed from the star counts were not, since stars below the detection limit of the SDSS would be excluded from the star counts. Using both data sets for the

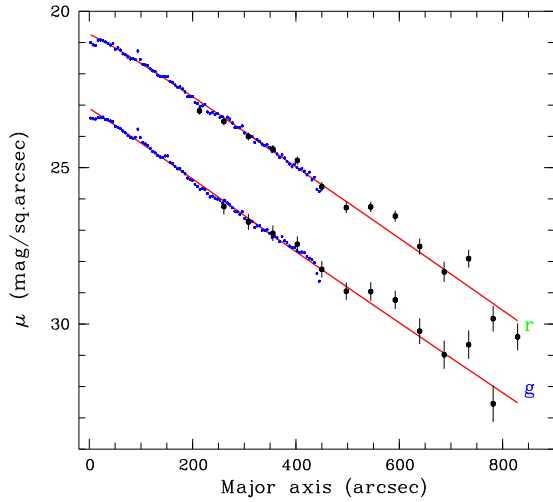


Figure 7. Composite SDSS gr -band SBPs. The SBPs were calculated in circular apertures for the unresolved part of the Pegasus dwarf irregular galaxy (blue points) and recalculated to the major axis using an ellipticity of $e=0.61$. The other data points for the SBP were calculated from star counts (black points) in ellipses with parameters taken from the best-fit model for the stellar surface density map and corrected for the part of the colour-magnitude diagram that is not detected in the SDSS data. The red curves represent the best-fit Sérsic model calculated from the SBPs for the unresolved inner part of Pegasus dwarf galaxy. The figures indicate that this model also fits the outer, fainter parts of this object reasonably well. The SBP profile for the r filter was shifted by an additional -2 magnitudes for clarity.

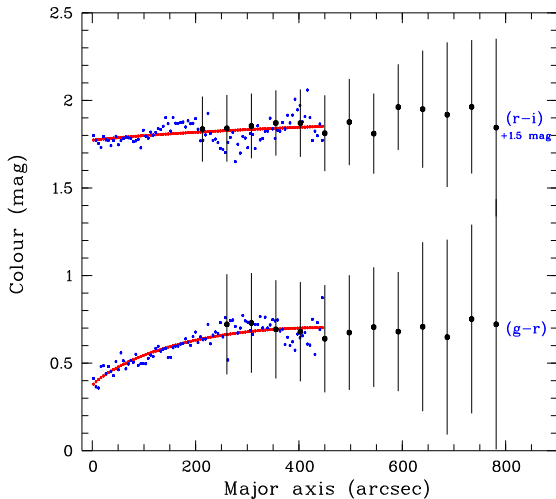


Figure 8. Composite SDSS $(g-r)$ and $(r-i)$ colour distributions. One of the components of the colour distributions was calculated in circular apertures for the unresolved part of PegDIG (blue points) and recalculated to the major axis using an ellipticity $e=0.61$. The other component was calculated from star counts (black points) in ellipses with parameters taken from the best-fit to the stellar surface density map and corrected for the undetected part of the colour-magnitude diagram. The red curves represent the best-fit Sérsic models that were calculated for the SBPs created for the unresolved part of Pegasus dwarf galaxy. The $(r-i)$ colour distribution was shifted by $+1.5$ magnitudes for clarity.

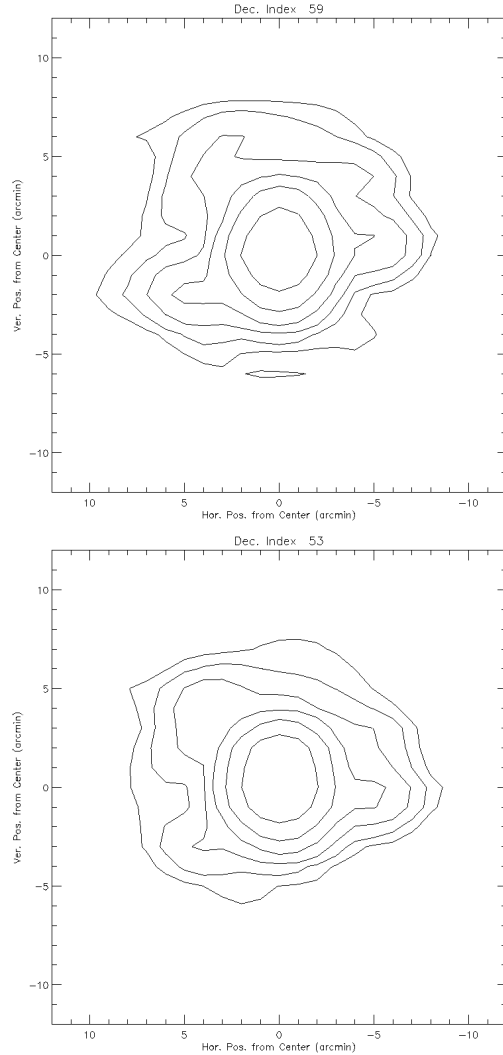


Figure 9. Effective ALFALFA beams at two representative declinations. Top shows declination $14^{\circ}47^m30^s$ and bottom shows $14^{\circ}41^m30^s$. The contours are spaced logarithmically, in steps of 3.33 dB down from the beam maximum.

part of the galaxy where the two methods overlap we can derive factors for the different filters and derive composite SBPs down to the faintest levels of PegDIG. These SBPs can be used to understand the evolutionary history of the galaxy, since the star formation in the outskirts of the galaxy presumably took place a long time ago.

The interpretation of these correction factors is that they compensate the SBPs in the galaxy part created by using resolved PegDIG stars for the missing light produced by the fainter stars that are not detected on SDSS images. The underlying assumption is that the slope and cutoffs of the IMF are constant between the inner unresolved part of PegDIG and the outer part where the brighter stars are resolved and recorded.

Composite SBPs in the gri bands were constructed from the unresolved part of the galaxy and from SBPs that were calculated from the star counts. Some of these composite SBPs are shown in Figure 7. Figure 8 shows the composite $(g-r)$ and $(r-i)$ colours. Both the $(g-r)$ and $(r-i)$

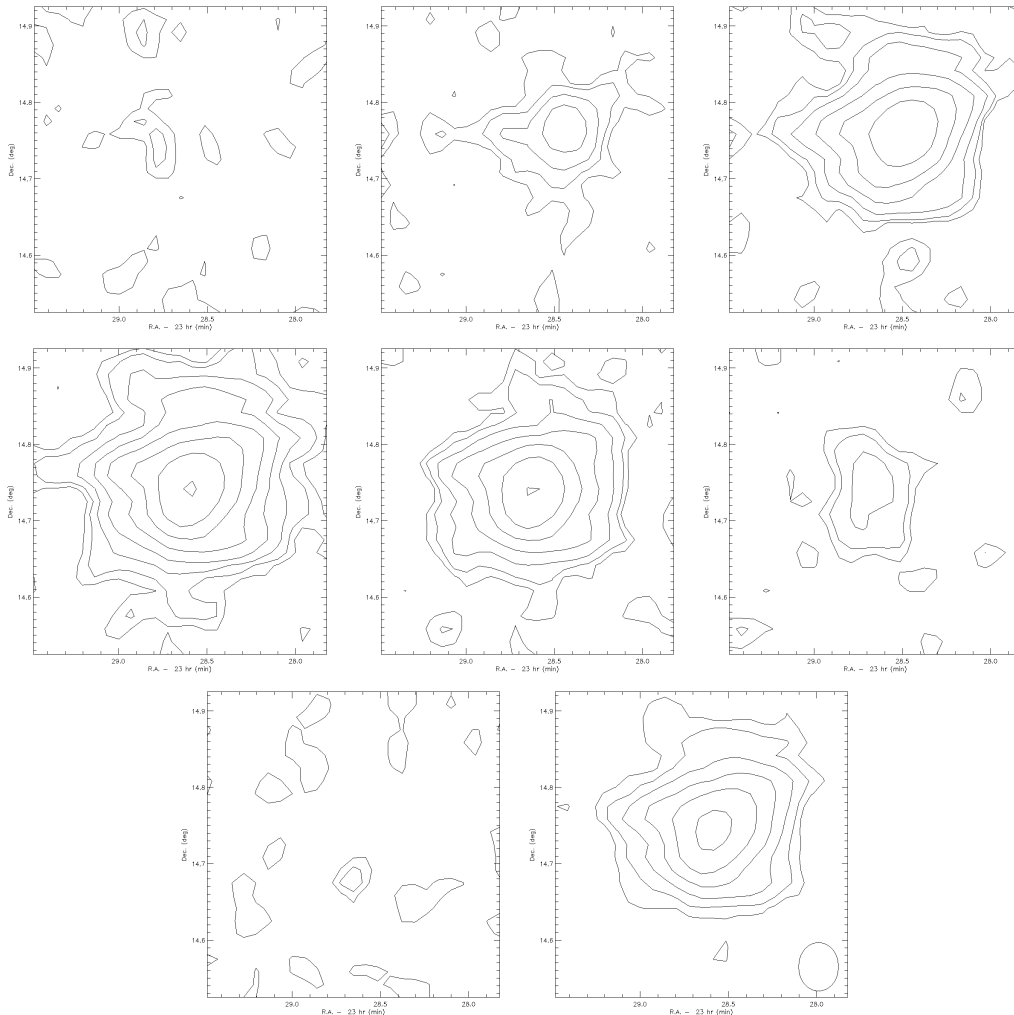


Figure 10. Channel maps of the HI distribution and the integrated HI of PegDIG, derived from the ALFALFA observations. The central velocities of each channel map are (from left to right) -138 , -153 , -169 km s^{-1} in the top row, -184 , -200 , -215 km s^{-1} in the middle row, and -231 km s^{-1} in the bottom row. The total HI map is shown in the bottom-right panel, which also displays the beam used to produce all the maps.

composite colours show very stable values for the outer parts of the galaxy, which justifies our previous statement.

The correction factors for the *gri* filters were estimated visually, using both the SBPs and the colour diagrams. Their final accuracy is presumably about ± 0.1 mag, since the colour diagrams are very sensitive to small photometric errors, and we estimate these to be ~ 0.05 mag for each band used here. The correction factors themselves are 2.25 mag for *g*, 1.85 mag for *r* and 1.65 mag for *i* filter. They were obtained by shifting vertically the values for the outer part of the galaxy to match those for the inner, unresolved part of PegDIG.

4 HI OBSERVATIONS

ALFALFA, the Arecibo Legacy Fast ALFA extragalactic HI survey (Giovanelli et al. 2005) is a blind neutral hydrogen survey that will ultimately cover 7074 square degrees of the high galactic latitude sky visible from Arecibo. It provides an extragalactic HI line spectral database covering the redshift

range between -1600 km s^{-1} and $18,000$ km s^{-1} . The “fall” part of the survey maps the sky region from $\text{RA}=22^h$ to 3^h over most of the declination range accessible from Arecibo ($\delta=0-36^\circ$). We collected the relevant HI observations covering PegDIG from the ALFALFA archives as a grid containing the galaxy. The ALFALFA observations are conducted at the Arecibo telescope with the 7-feed ALFA receiver. As described elsewhere (Giovanelli et al. 2005a, 2005b, 2007), data acquisition for ALFALFA is done in a fixed azimuth, drift-scan mode. Each surveyed sky region is covered by two partly-overlapping drift scans collected at two different epochs in order to sample at better than Nyquist spatial frequency.

The two scan passes are separated in time by several months, thus comparing the data from the two epochs helps in ruling out spurious detections. When data acquisition is completed over a given region of the sky, the individual drift scans are assembled and regridded to form three-dimensional data cubes or “grids”. These grids are $2.4^\circ \times 2.4^\circ$ in size with 1 arcmin sampling, and have 1024 channels along the spec-

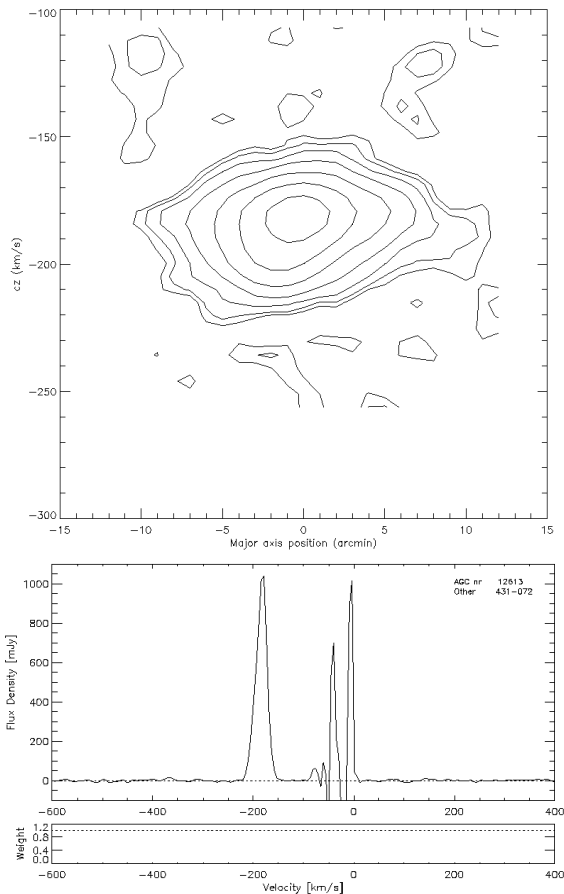


Figure 11. *Top panel:* Position-velocity contour map along the major axis of PegDIG. *Bottom panel:* The global spectrum (to the 100 mJy km s⁻¹ iso-intensity level) of PegDIG. The peaks between 0 and -100 km sec⁻¹ are Galactic hydrogen.

tral axis. Since the velocity resolution is ~ 5.3 km s⁻¹ (before Hanning smoothing), in order to cover the full ALFALFA velocity range which extends from -2000 to 18,000 km s⁻¹ each grid is separated into four redshift subgrids, covering the velocity ranges: -2000 – 3300 km s⁻¹, 2500 – 7900 km s⁻¹, 7200 – 12,800 km s⁻¹, and 12,100 – 17,900 km s⁻¹. For mapping the HI in PegDIG we used only the first velocity grid of the data cube at the PegDIG coordinates.

The central pixel of ALFA has low sidelobes, but the outer six pixels have significant coma lobes. Furthermore, the contributions of stray radiation and outer sidelobes to all the beams is not negligible. Data at each gridpoint in the ALFALFA grids are obtained by a weighted average of data from each beam that passes within a few arcmin from that point, thus the effective beam at any point has a quite complex shape. An IDL procedure for constructing effective beams for individual gridpoints from the beammaps of the seven separate beams (Irwin et al. 2009) was written by J. Dowell (Grossi et al. 2008). Using this procedure, we have constructed effective beams at each declination pixel in the grid. Two of these are shown in Figure 9.

The pronounced extensions shift in direction from one declination to another as little as 2' away as the dominant contribution to the received flux shifts from one ALFA pixel to the next. At a level of 10% of the main beam, these exten-

sions to the effective beams cause strong, extended sources like PegDIG to have apparent emission reaching a few arcmin beyond the edge of the actual HI distribution at any declination where one of these extensions stretches toward the position of peak emission from the galaxy.

Figure 10 shows the individual HI channel maps (averages of 3 ALFALFA velocity channels each) at the velocities -137.9, -153.4, -168.8, -184.3, -199.7, -215.1, and -230.6 km s⁻¹. The contours are drawn at 2.15, 4.64, 10.0, 21.5, 46.4, 100, 215, 464, and 1000 mJy. The bottom-right panel in Figure 10 presents the total HI map (integrated over velocity) with contour levels of 0.35, 0.74, 1.60, 3.5, 7.4 and 16.0 $\times 10^{19}$ atoms cm⁻². The ALFA beam used to produce these maps is plotted at the lower-right corner of the total HI map; this is a fairly elliptical beam elongated north-south, with major axes of 3'.3 \times 3'.9. The higher level contours agree well with the previous map of Hoffman et al. (1996) derived from Arecibo observations with the flat feed. The lower contours in our map show some differences, partly because the 1996 map was not a complete one with points spaced along major and minor axes as opposed to a full grid, and because the side-lobe structure is very different between the flat feed and the seven-feed ALFA.

From an inspection of the gridview display of the individual channels in Figure 10, we estimate that the structure in the lowest two contours to the north of the galaxy is possibly, as explained above, emission into the sidelobes of the beams that spanned that region and is probably spurious. The extensions to the east and southwest could also be sidelobe emission or could be real; this requires further observations.

The global spectrum (to the 100 mJy km s⁻¹ isophote level) for PegDIG, derived from the ALFALFA observations, is shown in the left panel of Figure 11. The systemic HI velocity is -183.6 km s⁻¹ and the width at 50% of the peak is 23.4 \pm 2.4 km s⁻¹. The corresponding quantities at 20% of the peak are -185.2 and 38.6 \pm 2.4 km s⁻¹. The HI profile is best-fitted by a Gaussian centred at -183.4 km s⁻¹ with FWHM=23.6 \pm 0.3 km s⁻¹. The total HI flux is 28.1 \pm 0.1 Jy km s⁻¹, or 27.83 \pm 0.06 Jy km s⁻¹ if the integral under the best-fit Gaussian is used. This corresponds to a total HI mass of 6.6 $\cdot 10^6$ M_⊙ at the 1 Mpc nominal distance. There are no visible high-velocity HI wings. Note also that the signal from PegDIG is clearly distinct from the Galactic emission between -100 and 0 km s⁻¹ at this velocity resolution.

Figure 11 shows the major axis position-velocity (PV) contour map of PegDIG. To produce it we rotated the declination (DEC) – right ascension (RA) maps by 25° (which we estimate to be the angle of the major axis of the HI distribution away from the RA axis), then summed along the minor axis. The result is plotted as a contour map in the position vs. velocity plane, with contour levels 21.544, 46.416, 100.0, 215.44, 464.16, 1000.0, and 2154.4 mJy. The lowest two levels show the effects of the coma lobes, but the rest of the contours should be robust. The PV map indicates a solid-body rotation curve with opposite ends differing by 15 km s⁻¹, with a stream to more negative *cz* about 5 arcmin from the centre of the galaxy. The positive direction of the position axis is toward the SE.

We measured a flux integral similar to that of Young et al. (2003) and almost twice that measured by Sill & Israel (2002). We conclude that, to a level of 2 mJy/beam, the

galaxy is 0.3 degrees wide in RA and 0.25 degrees in DEC. The peak of the HI is at RA = $23^h 28^m 55^s$, DEC $+14.75^\circ$ in J2000 coordinates and at about -184 km s^{-1} . The FWHM of the HI line is about 28 km s^{-1} , about 10% wider than the width derived by Young et al. The HI distribution does not show an obvious compression ridge to the SE, or a tail to the NW smoothed out by our wide beam. The slight crowding of the contours to the SE of the total HI distribution and slight elongation to the NW may be indicative of the compression ridge and tail inferred by Young et al. (2003) from their VLA map, but lacking a procedure to deconvolve the multiple asymmetric beams from the map we cannot be certain. However, we do not see any extension of the HI significantly beyond the outermost Young et al. contour even though ALFALFA is sensitive to column densities 4 or 5 times lower than the sensitivity limit of the Young et al. map.

5 THE STELLAR POPULATIONS

van Zee (2000) presented B and $(U - B)$, $(B - V)$ profiles that extend only ~ 300 arcsec from the centre; these show that the stellar population changes from $(B - V) \simeq 0.6$ one arcmin from the centre ($\mu_B \simeq 24$) to ~ 0.8 some four arcmin from the centre. This is similar to the colour gradient found here for the unresolved part of the galaxy.

Hierarchical galaxy formation scenarios predict that dwarf galaxies should show traces of an old stellar population. And indeed, all nearby dwarf galaxies show clear evidence for the presence of old stellar populations (Grebbe & Gallagher 2004), i.e., populations older than 10 Gyr, as traced by, e.g., the presence of a horizontal branch. This may also be the case for PegDIG, where traces of present-day very low level star formation ($4.4 \times 10^{-5} M_\odot \text{ yr}^{-1}$) were found (e.g., Hunter & Elmegreen 2004) while most of the stars belong to earlier generations. Indeed, the deepest existing HST data show clear evidence for substantial populations with ages of 9 Gyr and younger as traced by a very prominent red clump (Gallagher et al. 1998). Those data approach the detection limit just below the intermediate-age red clump, making it very difficult to establish the presence of a horizontal branch (although there are indications of a density enhancement in the corresponding region in the colour-magnitude diagram in Fig. 15 of Gallagher et al. 1998).

van Zee (2000) found that PegDIG had the reddest $(U - B)$ and $(B - V)$ colours of all the galaxies in her sample. She could not fit these with a constant star formation model, but could fit them with a continuous but declining star formation rate, or with an aging, a few Gyr old starburst. She proposed that the very low star formation rate, now relegated to the innermost parts of the galaxy, might result from the depletion of the galaxy's HI reservoir. van Zee (2000) mentioned also that the HII regions detected in her $H\alpha$ images are so faint that they would not have been detected if PegDIG were more distant.

To estimate the distribution of stellar population ages in PegDIG, we compared the derived integrated colours in its different parts with model tracks from the PEGASE2 package (Fioc & Rocca-Volmerange 1999) for metallicity values of $z=0.02$ (solar), $z=0.008$ (1/3 of solar) and $z=0.004$

(1/5 of solar). Since the photometric systems (u', g', r', i', z') used for the calculations of PEGASE2 evolutionary tracks and (u, g, r, i, z) used in the real SDSS observations are slightly different, we applied the transformation formulae from Tucker et al. (2006) in order to correct theoretical values to the (u, g, r, i, z) system. PegDIG has been found to have a low present-day ISM metallicity of $\sim 1/5$ of solar (Skillman, Bomans & Kobulnicky 1997) and possibly has more metal-poor older stars (Gallagher et al. 1998). Based on the models we used, tracks of even lower metallicities ($< 1/5$ of solar) would not match the red colours observed in the outer parts of PegDIG and thus these tracks are not plotted.

In Fig. 12 we plot model tracks of colour evolution in the $(g-r)_0$ versus $(u-g)_0$ and $(r-i)_0$ versus $(g-r)_0$ diagram for a standard Salpeter IMF, with lower and upper mass cutoff limits of 0.1 and $120 M_\odot$. All observed colours are corrected for Milky Way foreground extinction. Different tracks in Fig. 12 represent the colour evolution for continuous SF with constant SFR (dashed lines) and for an aging instantaneous SF episode (solid lines) as two extremes of all possible SF histories. The hexagons on the evolutionary tracks with the respective numbers mark ages in Gyr since the beginning of SF.

We seek to constrain the mean age of the dominant population in different annuli by trying to fit simultaneously both colour-colour plots, the $(u-g)_0$ vs. $(g-r)_0$ and the $(g-r)_0$ vs. $(r-i)_0$ colours. Clearly, younger populations are more prominent in the central regions, where the mean colours agree relatively well with the 1 Gyr tracks. In the outermost regions the averaged age is 5–10 Gyr or less. Our data do not allow us to prove or to disprove the presence of an old population (older than 10 Gyr), but the comparison of the integrated colours with population synthesis models suggests that the contribution of such an old population to the integrated light is fairly minor. Hence the colour gradient appears to be consistent with an age gradient in the sense that younger populations are more centrally concentrated, while older populations show a more extended distribution. Of course, independent of the integrated colours, we know already from published earlier studies that an age gradient is present, as indicated by, e.g., the centralised distribution of the HII regions.

As is well-known, colour gradients may be caused by either age, metallicity, or reddening gradients (Harbeck et al. 2001; Hunter & Elmegreen 2006). We cannot unambiguously disentangle these three effects in our data, but we can at least attempt to qualitatively comment on their importance. Since the intrinsic reddening of PegDIG seems to be low (Krienke & Hodge 2001), we discard extinction as a significant contributor to the observed colour gradients. We have insufficient data to constrain a potential metallicity gradient, but we note that the slope of the metallicity gradient has to have an opposite sign to the observable one: the more metal-poor track has bluer colours compared to the more metal-rich track. In other dwarf galaxies for which more detailed data are available, metallicity gradients tend to be small despite considerable scatter at a given age (e.g., Kniazev et al. 2005; Glatt et al. 2008; Koch et al. 2006). Altogether, it seems likely that our large-scale colour gradients are indeed primarily driven by age, although an age gradient may certainly also be linked with a metallicity gradient.

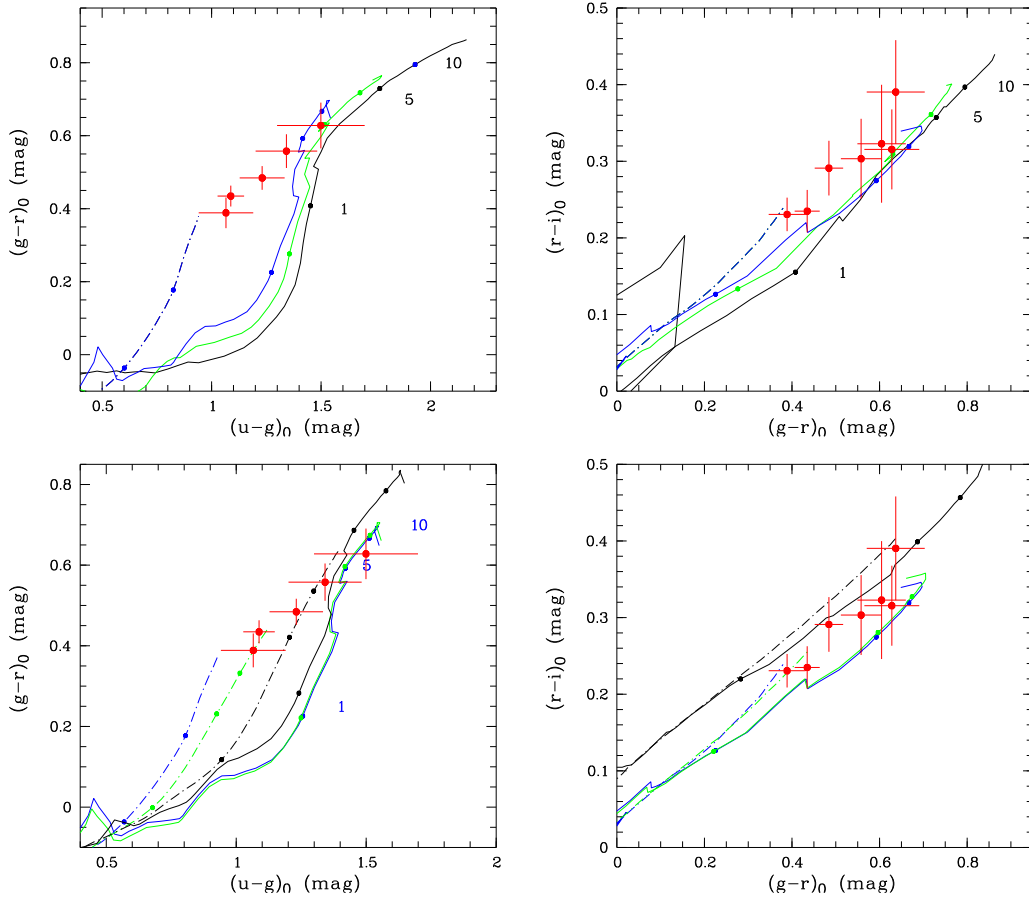


Figure 12. Two-colour diagrams with theoretical tracks from PEGASE2 for evolving stellar populations. The observed colours are corrected for Milky Way foreground extinction and are shown as red filled circles with error bars for the following major axis distances: 0–50, 50–100, 100–150, 150–250, 250–400, 400–600 and 600–800 arcsec. $(u-g)_0$ could be only calculated up to a major axis distance of 400 arcsec. The observed colours were averaged inside each major axis distance bin and the $\pm 1\sigma$ errors also reflect the scatter of colour in each distance range. Redder colours correspond to an increased major axis distance: the lowest-leftmost point represents the centre of PegDIG and highest-rightmost one corresponds to the outermost part. *Top panels:* Tracks with a standard Salpeter IMF, for instantaneous (solid) and continuous (dashed line) SF laws using different metallicities: blue – $z=0.004$ ($1/5 Z_{\odot}$), green – $z=0.008$ ($1/3 Z_{\odot}$) and black – Z_{\odot} . Filled black hexagons along the tracks, with respective numbers, mark the time since the beginning of SF: 1, 5 and 10 Gyr. *Bottom panels:* Tracks for instantaneous (solid) and continuous (dashed line) SF laws with a standard Salpeter IMF (blue) for $z=0.004$ and non-standard Salpeter IMFs: slope is -1.6 for green and -2.85 for black.

Population gradients have been identified in early-type and late-type dwarf galaxies alike (e.g. Harbeck et al. 2001; Parodi et al. 2002; Makarova et al. 2002, 2005; Lisker et al. 2006; Hunter & Elmegreen 2006), although not all dwarf galaxies show such gradients. Generally seen as colour gradients, such variations are usually interpreted as age gradients. They appear to indicate longer-lasting star formation in the deeper, inner parts of the potential well where the star-forming material accumulates more easily and/or can be retained more easily. PegDIG seems to fit this trend as well.

6 DISCUSSION

One of the results of the present work is the derivation of surface brightness profiles for PegDIG that extend about 1.6 times further out than what was found in previous surface photometry studies (Tikhonov 2006a). Other deep optical surveys of dIrrs in the Local Group

have found additional evidence for stellar distributions much more extended than previously thought: e.g., NGC 6822 (de Blok & Walter 2006), Leo A (Vansevicius et al. 2004), and IC 1613 (Battinelli et al. 2007). Tikhonov (2005, 2006b) also found such an effect for many nearby face-on and edge-on dIrrs.

Our deep surface photometry, using stars identified as belonging to PegDIG and eliminating Milky Way stars in the foreground, showed that it is possible to fit a Sérsic surface brightness distribution to the galaxy at least to a radius of $14 \text{ arcmin} \simeq 4 \text{ kpc}$. The stellar distribution shows some concentrations around the unresolved 2 kpc part, and some irregular extensions at the NW end of the major axis. Note that this region shows less HI than the SE part, when our maps are compared with those for neutral hydrogen from Young et al. (2003). The HI column density shown in their Fig. 5 has a peak of $\sim 10^{21} \text{ atoms cm}^{-2}$ at RA = $23^{\text{h}} 28^{\text{m}} 35^{\text{s}}$, DEC = $+14^{\circ} 44^{\text{m}} 15^{\text{s}}$, identical to the peak of the ALFALFA maps.

Our results allow the derivation of some general properties of PegDIG. The total HI flux and the total B magnitude yield $M(\text{HI})/L_B \simeq 0.4$. A rough estimate of the total dynamical mass can be derived from the PV plot in the left panel of Figure 11. Assuming that the outermost gaseous regions of PegDIG rotate with $\sim 60 \text{ km s}^{-1}$ at a galactocentric distance of 4 kpc, the total dynamical mass is $M_{dyn} \simeq 3.3 \times 10^8 M_\odot$. The neutral hydrogen contributes only 2% of this mass. The mass in stars can be roughly estimated from the SDSS colours plotted in Figure 12; these correspond to main-sequence K stars. If the light were produced solely by K5 stars, the total mass in stars would be $M_* = 1 \times 10^8 M_\odot$, about 30% of the total dynamical mass. This indicates that while PegDIG has a significant amount of dark matter, it is not a dark-matter-dominated galaxy, contrary to the assertion of Aparicio et al. (1997).

Wilkinson et al. (2004) interpreted the sharp drop in the surface brightness profile of the Draco dSph as the signature of a kinematically cold stellar population in the outer parts of the galaxy. They proposed two possible explanations for this phenomenon, which they presented along with arguments against accepting them. One is a two-population model with a hot bulge and a cold disk or halo that does not fit either the observed kinematics nor the light distribution. The other is tidal reshaping by the Milky Way galaxy, which requires very tight constraints on the orbit of the dwarf galaxy. We mention this here since a similar phenomenon may be present in PegDIG, even though PegDIG is more than five times as distant from the nearest massive spiral as the Draco dSph (Grebel et al. 2003).

Karachentsev et al. (2004) mentioned that the major disturber galaxy for PegDIG, in terms of tidal interactions, is M31, with a θ parameter of 1.2. This parameter is the tidal index, which is defined as:

$$\theta_i = \max[\log \frac{M_k}{(D_{ik})^3}] + C \quad (5)$$

Here i is the index of the specific galaxy θ is calculated for, k is the index of any other galaxy, M_k is the mass of the k -th galaxy and D_{ik} is the 3D space distance between the i -th and the k -th galaxy (Karachentsev & Makarov 1999). Galaxies with $\theta \leq 0$ can be considered to be undisturbed, while objects with $\theta \geq 5$ are considered to be highly disturbed. Based on the calculated value, PegDIG could be somewhat affected by M31, but not by an extreme tidal interaction. Hunter & Elmegreen (2004) listed M31 as the nearest neighbour to PegDIG, at a projected distance of 450 kpc and a relative recession velocity of $+117 \text{ km sec}^{-1}$. Note though that since the actual orbit of PegDIG is not known, and it could even be on a fairly radial orbit around M31, a relatively strong tidal interaction in the past cannot be excluded.

McConnachie et al. (2007) plotted some of the PegDIG neighbours in their Fig. 1 (lower right panel). Their argument is that a comparison of the HI contours with the stellar distribution fits a morphology of gas being stripped away by ram pressure. They identify a “compression front” on the SE end of the galaxy. In order for ram pressure stripping to take place, they require the Local Group to be filled by a tenuous ($\sim 10^{-5} \text{ cm}^{-3}$), rather warm ($\sim 10^5 \text{ K}$) gaseous medium. Ram pressure stripping would also modify the gas distribution in and around the galaxy. In fact, this is the

main argument used by McConnachie et al. in bringing up the stripping possibility. The morphological modifications that should appear if the ram pressure stripping argument is valid are a leading edge compression region and the creation of a tail of stripped material following the galaxy.

The deep HI maps shown in Figure 10 lack the signatures of either a strong tidal interaction or of ram pressure stripping of the gas from the galaxy. On the contrary, the low column density gas observed at the outskirts of PegDIG and the lack of disturbances in the distribution of this tenuous gas imply that any presumed interaction with an intergalactic medium, as proposed by McConnachie et al (2007), can probably be discounted. Grebel et al. (2003) presented simple estimates of the efficiency of ram pressure stripping by a homogeneous Local Group intergalactic medium and concluded that the densities are too low to have a noticeable effect. However, Grebel et al. (2003) also argued that a putative *clumpy* medium could be rather effective. But the absence of disturbances in the PegDIG HI contours does not support stripping by a clumpy intergalactic medium.

With the present star formation rate derived by Young et al. (2003) and the total HI mass measured in this work, the star formation could last for another 2×10^{11} years. Such slow, continuous star formation extending over a Hubble time or more is typical for dIrr galaxies (e.g. Hunter & Gallagher 1986; van Zee 2001). The central HI column density is a bit short of the canonical threshold for star formation, but this canonical limit is not always valid for low-mass galaxies (e.g., Hunter et al. 1998). Is it possible that we are seeing PegDIG during an extended lull in star formation, while the gas is settling back after having been distended by, e.g., supernovae in the last star formation episode, akin to scenarios described by, e.g., Dong et al. (2003)? Amplitude variations in the intensity of star formation are commonly observed in dIrr galaxies, so here also PegDIG would conform to the typical properties of these objects (e.g., Tosi et al. 1991; Grebel 1997).

Begum et al. (2006) discussed the SF threshold in very faint low-mass galaxies based on synthesis observations with the Giant Metrewave Radio Telescope (GMRT). They found that while current star formation (as traced by $\text{H}\alpha$ emission) is confined to regions with relatively large HI column density [$N_{\text{HI}} > (0.4-1.7) \times 10^{21} \text{ cm}^{-2}$], the morphology of the $\text{H}\alpha$ emission is generally not correlated with that of the high HI column density gas. A high gas column density may be a necessary condition for star formation, but it is not sufficient, for their sample at least, to ensure that star formation does in fact occur.

We can also rule out tidal deformation, since such distortions are expected to be symmetric with respect to the centre, while for PegDIG any distortions are relegated to the NW side. Our findings imply that PegDIG might be a recent acquisition of the Local Group, now in the outskirts of the LG and far away from any nearby massive galaxies, that was formed in a comparatively empty region without major disturbers. However, without knowledge of its orbit we cannot rule out past interactions with M31.

7 CONCLUSIONS

We analysed images of the Pegasus dwarf irregular galaxy collected by the SDSS survey and found that the unresolved part can be fitted by a Sérsic intensity profile down to ~ 30 mag arcsec $^{-2}$. Using very effective filtering in the colour-magnitude space of SDSS data, we reduced the contamination by foreground Galactic field stars and significantly increased the contrast for the outer part of the Pegasus dwarf where we identified resolved stars that belong to PegDIG. This allowed the extension of the surface photometry to much fainter levels.

Our extended surface photometry, reaching down to a surface brightness of $\mu_g \simeq 33$ mag arcsec $^{-2}$, revealed a ~ 8 kpc wide stellar distribution following the same Sérsic profile as found for the unresolved part, composed of a stellar population similar to that in the ~ 2 kpc main body, but significantly older. The distribution of colours across the galaxy body shows that the innermost parts of the galaxy contain the youngest population. A comparison to population synthesis models suggests a mean age of ~ 1 Gyr for this part, and we know from earlier work at HST resolution that the youngest stars have ages of only a few 10 Myr. The outermost parts of PegDIG are much older with a mean age from integrated colours of at least 5 Gyr, indicating that there the contribution of younger populations is comparatively small. The total dynamical mass of the galaxy is $\sim 3 \times 10^8 M_\odot$, of which about 30% is in stars and only 2% is in HI.

We found that the stellar distribution of PegDIG is considerably more extended than previously thought. Mapping the HI distribution to very low column density levels at Arecibo revealed that the hydrogen distribution is slightly smaller than that of the stars revealed by the present study. PegDIG is therefore yet another dIrr where the HI is not much more extended than the stellar distribution, as it used to be in the classical picture of dIrrs.

Our deep HI map shows an extended and fairly regular gas distribution with solid-body-like rotation. We do not observe low column density tails extending beyond the edges of the neutral gas distribution shown in earlier synthesis array images (Young et al. 2003). Tidal stripping therefore seems unlikely. On the basis of the HI observations alone, we cannot rule out ram pressure interaction with extragalactic gas, and the relatively small extent of the HI vis-a-vis the distribution of stars may even support the hypothesis that the outermost gas has been stripped.

We identified faint extensions of the optical light distribution of PegDIG at the north-west end that do not follow the expected distortions caused by a tidal interaction. We also showed that a number of stellar concentrations – possibly extended stellar associations – are located around the unresolved central galaxy body. Rings of stellar associations have been found in a number of dIrrs and could be a possible sign of outward-propagating star formation but, on the other hand, PegDIG also has very young stars in its innermost regions as shown by the HST data (Gallagher et al. 1998).

ACKNOWLEDGMENTS

We thank the anonymous referee for comments that improved the presentation of the manuscript. This paper makes

extensive use of SDSS data products. Funding for the SDSS and SDSS-II has been provided by the Alfred P. Sloan Foundation, the Participating Institutions, the National Science Foundation, the U.S. Department of Energy, the National Aeronautics and Space Administration, the Japanese Monbukagakusho, the Max Planck Society, and the Higher Education Funding Council for England. The SDSS Web Site is <http://www.sdss.org/>.

The SDSS is managed by the Astrophysical Research Consortium for the Participating Institutions. The Participating Institutions are the American Museum of Natural History, Astrophysical Institute Potsdam, University of Basel, University of Cambridge, Case Western Reserve University, University of Chicago, Drexel University, Fermilab, the Institute for Advanced Study, the Japan Participation Group, Johns Hopkins University, the Joint Institute for Nuclear Astrophysics, the Kavli Institute for Particle Astrophysics and Cosmology, the Korean Scientist Group, the Chinese Academy of Sciences (LAMOST), Los Alamos National Laboratory, the Max-Planck-Institute for Astronomy (MPIA), the Max-Planck-Institute for Astrophysics (MPA), New Mexico State University, Ohio State University, University of Pittsburgh, University of Portsmouth, Princeton University, the United States Naval Observatory, and the University of Washington.

This work is based in part on observations collected at Arecibo Observatory. The Arecibo Observatory is part of the National Astronomy and Ionosphere Center, which is operated by Cornell University under a cooperative agreement with the National Science Foundation.

This research has made use of the NASA/IPAC Extragalactic Database (NED) which is operated by the Jet Propulsion Laboratory, California Institute of Technology, under contract with the National Aeronautics and Space Administration. Moreover, this research has made extensive use of NASA's Astrophysics Data System.

REFERENCES

- Adelman-McCarthy J.K., et al., 2007, *ApJS*, 172, 634
- Aparicio A., 1994, *ApJ*, 437, L27
- Aparicio A., Gallart C., Bertelli G., 1997, *AJ*, 114, 669
- Aparicio A., Tikhonov N., Karachentsev I., 2000, *AJ*, 119, 177
- Armandroff T. E., Jacoby G. H., & Davies J. E. 1999, *AJ*, 118, 1220
- Battinelli P., Demers S., & Artigau É. 2007, *A&A*, 466, 875
- Begum A., Chengalur J. N., Karachentsev I. D., Kaisin S. S., Sharina M. E., 2006, *MNRAS*, 365, 1220
- Bell E. F., et al. 2008, *ApJ*, 680, 295
- Belokurov V., et al. 2006, *ApJ*, 647, L111
- Belokurov V., et al. 2007a, *ApJ*, 658, 337
- Belokurov V., et al. 2007b, *ApJ*, 654, 897
- Christian C. A., Tully R. B., 1983, *AJ*, 88, 934
- Coleman M. G., Jordi K., Rix H.-W., Grebel E. K., Koch A. 2007, *AJ*, 134, 1938
- Courteau S., van den Bergh S. 1999, *AJ*, 118, 337
- de Blok W. J. G., Walter F. 2006, *AJ*, 131, 343
- de Vaucouleurs G., 1975, *SSS*, 9, 557
- Dohm-Palmer R. C., et al., 1998, *AJ*, 116, 1227
- Dong S., Lin D. N. C., Murray S. D. 2003, *ApJ*, 596, 930

- Fioc M., & Rocca-Volmerange B. 1999, arXiv:astro-ph/9912179
- Fisher J. R., Tully R. B., 1975, *A&A*, 44, 151
- Fisher J. R., Tully R. B., 1979, *AJ*, 84, 62
- Gallagher J. S., Tolstoy E., Dohm-Palmer R. C., Skillman E. D., Cole A. A., Hoessel J. G., Saha A., Mateo M., 1998, *AJ*, 115, 1869
- Gilmore G., Wilkinson M. I., Wyse R. F. G., Kleyna J. T., Koch A., Evans N. W., Grebel E. K., 2007, *ApJ*, 663, 948
- Giovanelli R., et al. 2005, *AJ*, 130, 2598
- Glatt K., et al., 2008, *AJ*, 135, 1703
- Gnedin N. Y., Kravtsov A. V., 2006, *ApJ*, 645, 1054
- Grebel E.K., 1997, *Reviews in Modern Astronomy*, 10, 21
- Grebel E.K., 2001, *Ap&SSS*, 277, 231
- Grebel E. K., Guhathakurta P., 1999, *ApJ*, 511, L101
- Grebel E.K., Gallagher J.S., Harbeck D., 2003, *AJ*, 125, 1926
- Grebel E. K., Gallagher J. S., 2004, *ApJ*, 610, L89
- Greggio L., Marconi G., Tosi M., Focardi P., 1993, *AJ*, 105, 894
- Grillmair C.J., Freeman K.C., Irwin M., Quinn P.J., 1995, *AJ*, 109, 1553
- Grossi, M., et al. 2008, *A&A*, 487, 161
- Harbeck D., et al., 2001, *AJ*, 122, 3092
- Haynes M., et al. 2008, in *The Evolution of Galaxies Through the Neutral Hydrogen Window*, AIP Conf. Proc., ed. R. Minchin & E. Momjian, in press (arXiv:0806.1670)
- Hoessel J.G., Mould J.R., 1982, *ApJ*, 254, 38
- Hoessel J.G., Abbott M.J., Saha A., Mossman A.E., Danielson G.E., 1990, *AJ*, 100, 1151
- Hoffman G. L., Salpeter E. E., Farhat B., Roos T., Williams H., Helou G., 1996, *ApJS*, 105, 269
- Hogg D.W., Finkbeiner D.P., Schlegel D.J., Gunn J.E., 2001, *AJ*, 122, 2129
- Hunter D. A., Gallagher J. S., 1986, *PASP*, 98, 5
- Hunter D. A., Elmegreen B. G., Baker A. L., 1998, *ApJ*, 493, 595
- Hunter D. A., Elmegreen B. G., 2004, *AJ*, 128, 2170
- Hunter D. A., Elmegreen B. G., 2006, *ApJS*, 162, 49
- Ibata R.A., Gilmore G., Irwin M.J., 1994, *Nature*, 370, 194
- Ibata R., Irwin M., Lewis G., Ferguson A. M. N., Tanvir N., 2001, *Nature*, 412, 49
- Irwin, J.A., et al. 2009, *ApJ*, 692, 1447
- Jackson D. C., Cannon J. M., Skillman E. D., Lee H., Gehrz R. D., Woodward C. E., Polomski E., 2006, *ApJ*, 646, 192
- Jacoby G. H., Lesser M. P., 1981, *AJ*, 86, 185
- Jordi K., Grebel E.K., Ammon K., 2006, *A&A*, 460, 339
- Karachentsev I. D., Karachentseva V. E. 1999, *A&A*, 341, 355
- Karachentsev I. D., Makarov D. I., 1999, *IAUS*, 186, 109
- Karachentsev I. D., Karachentseva V. E., Huchtmeier W. K., 2001, *A&A*, 366, 428
- Karachentsev I. D., et al. 2002a, *A&A*, 383, 125
- Karachentsev I. D., et al. 2002b, *A&A*, 385, 21
- Karachentsev I. D., et al. 2002c, *A&A*, 389, 812
- Karachentsev I. D., et al. 2003, *A&A*, 408, 111
- Karachentsev I. D., Karachentseva V. E., Huchtmeier W. K., Makarov D. I., 2004, *AJ*, 127, 2031
- Kniazev A.Y., Grebel E.K., Pustilnik S.A., Pramskij A.G., Kniazeva T.F., Prada F., Harbeck D. 2004, *AJ*, 127, 704
- Kniazev A. Y., Grebel E. K., Pustilnik S. A., Pramskij A. G., Zucker D., 2005, *AJ*, 130, 1558
- Krienke K., Hodge P.W. 2001, *PASP*, 113, 1115
- Koch A., Grebel E. K., Wyse R. F. G., Kleyna J. T., Wilkinson M. I., Harbeck D. R., Gilmore G. F., Evans N. W., 2006, *AJ*, 131, 895
- Lee M. G., 1995, *JKAS*, 28, 169
- Lisker T., Glatt K., Westera P., Grebel E. K., 2006, *AJ*, 132, 2432
- Lo K. Y., Sargent W. L. W., Young K., 1993, *AJ*, 106, 507
- Lupton R., Gunn J.E., Ivezić Z., Knapp G.R., Kent S., Yasuda N. 2001, in *Astronomical Data Analysis Software and Systems X*, ASP Conf. Ser. 238, eds. F. R. Harnden, Jr., F. A. Primini, & H. E. Payne (San Francisco: ASP), 269
- Makarova L. N., Karachentsev I. D., Grebel E. K., Barsunova O. Y., 2002, *A&A*, 384, 72
- Makarova L. N., Karachentsev I. D., Grebel E. K., Harbeck D., Korotkova G. G., Geisler D., 2005, *A&A*, 433, 751
- Martin N. F., de Jong J. T. A., Rix H.-W., 2008, *ApJ*, 684, 1075
- Mateo M. L., 1998, *ARA&A*, 36, 435
- McConnachie A. W., Irwin M. J., Ferguson A. M. N., Ibata R. A., Lewis G. F., Tanvir N., 2005, *MNRAS*, 356, 979
- McConnachie A. W., Irwin M. J., 2006, *MNRAS*, 365, 1263
- McConnachie, A.W., Venn, K.A., Irwing, M.J., Young, L.M. & Geehan, J.J., 2007, *ApJ*, 671, L33
- Meschin I., Gallart C., Aparicio A., Cassisi S., Rosenberg A., 2009, *AJ*, 137, 3619
- Odenkirchen M. et al. 2001a, *ApJ*, 548, L165
- Odenkirchen M. et al. 2001b, *AJ*, 122, 2538
- Parodi B. R., Barazza F. D., Binggeli B., 2002, *A&A*, 388, 29
- Peng C.Y., Ho L.C., Impey C.D., Rix H., 2002, *AJ*, 124, 266
- Rockosi C. M., et al., 2002, *AJ*, 124, 349
- Sérsic J.L., 1968, *Atlas de Galaxies Australes*, (Cordoba, Argentina: Observatorio Astronomico)
- Schlegel D.J., Finkbeiner D.P., Douglas M., 1998, *ApJ*, 500, 525
- Skillman E. D., Bomans D. J., Kobulnicky H. A., 1997, *ApJ*, 474, 205
- Smolčić V., Zucker D. B., Bell E. F., Coleman M. G., Rix H. W., Schinnerer E., Ivezić Ž., Kniazev A., 2007, *AJ*, 134, 1901
- Stil J. M., Israel F. P., 2002, *A&A*, 389, 29
- Stoughton C., et al., 2002, *AJ*, 123, 485
- Tikhonov N. A., 2005, *Astronomy Reports*, 49, 501
- Tikhonov N. A., 2006a, *Astronomy Letters*, 32, 149
- Tikhonov N. A., 2006b, *Astronomy Reports*, 50, 517
- Tosi M., Greggio L., Marconi G., Focardi P., 1991, *AJ*, 102, 951
- Trujillo I., Graham A. W., Caon N., 2001, *MNRAS*, 326, 869
- Tucker D.L., Kent S., Richmond M.W., et al., 2006, *AN*, 327, 821
- van den Bergh S., 2000, *PASP*, 112, 529
- van Zee L., 2000, *AJ*, 119, 2757
- van Zee L., 2001, *AJ*, 121, 2003
- Vansevičius V., et al., 2004, *ApJ*, 611, L93
- Wilkinson M. I., Kleyna J. T., Evans N. W., Gilmore G. F., Irwin M. J., Grebel E. K., 2004, *ApJ*, 611, L21
- Willman B., et al., 2002, *AJ*, 124, 2600
- Willman B., et al., 2005, *ApJ*, 626, L85

- Yanny B., et al., 2003, ApJ, 588, 824
York, D.G., Adelman, J., Anderson J.E. et al., 2000, AJ,
120, 1579
Young L. M., van Zee L., Lo K. Y., Dohm-Palmer R. C.,
Beierle M. E., 2003, ApJ, 592, 111
Zucker D. B., et al., 2004, ApJ, 612, L117
Zucker, D. B., et al., 2004, ApJ, 612, L121
Zucker, D. B., et al., 2006, ApJ, 650, L41
Zucker, D. B., et al., 2007, ApJ, 659, L21

This paper has been typeset from a \TeX / \LaTeX file prepared
by the author.